Molecular Dynamics Simulations of the Phosphodiester-Linked Repeating Units of the *Haemophilus influenzae* Types c and f Capsular Polysaccharides

Christer Höög,[†] Aatto Laaksonen,[‡] and Göran Widmalm*,[†]

Department of Organic Chemistry and Division of Physical Chemistry, Arrhenius Laboratory, Stockholm University, S-106 91 Stockholm, Sweden

Received: November 9, 2000; In Final Form: May 2, 2001

The three-dimensional structure of the repeating units of *Haemophilus influenzae* types c and f capsular polysaccharides (CPS) have been investigated by molecular dynamics simulations. The models consist of disaccharides joined by phosphodiester linkages, explicit water, and sodium as the counterion. Four 1 ns simulations were performed for each type, with either different starting conformations or different methods to handle long-range truncation effects, namely, Ewald summation or force shift truncation. For the average properties investigated, the choice of the method did not make any significant difference. Limited flexibility was observed close to the sugar residues, whereas at the phosphorus atom, the torsions showed major transitions. For comparison, $^3J_{H,P}$ was measured on CPS material. On the basis of these spin−spin couplings, only small changes are required in the models of the disaccharide repeating unit to agree with data on the CPS. In addition, hydrogen bonding and radial and spatial distribution functions were analyzed to obtain a picture of solvent ordering around the disaccharides.

Introduction

Haemophilus influenzae is a Gram-negative bacterium causing, inter alia, meningitis, pneumoniae, and otitis. There are six serotypes (a−f) that carry a specific capsular polysaccharide.[1,2] Four of these (a, b, c, and f) are of the teichoic acid type, and two (a and b) have a ribitol phosphodiester in the repeating unit. Serotype b causes the most severe infections, especially in infants. However, today there are conjugate vaccines which induces a protective immune response to such infections.[3] There are also nonencapsulated ("non-typable") *H. influenzae* strains that cause less severe infections.[4]

Serotypes c[5,6] and f[7,8] contain disaccharide repeating units linked via phosphodiesters. The saccharide part is for type c −4-*β*-D-Glc*p*NAc3Ac-(1→3)-α-D-Gal*p*-1− and for type f −3-*β*-D-Gal*p*NAc-(1→4)-α-D-Gal*p*NAc3Ac-1−. Since these CPS's are joined by phosphodiester linkages having only two sugar residues per repeating unit, the degree of phosphodiester groups is large in comparison to those of many polysaccharides which do not carry these types of linkages in the backbone chain. However, there are reports of other pathogenic bacteria having phosphodiesters in the polymeric backbone, e.g., the CPS of *Streptococcus pneumoniae* type 7B[9] and the O-antigen part of the lipopolysaccharide from *Escherichia coli* O173,[10] but these polymers have seven and five sugars in their repeating units, respectively.

Saccharides being linked via phosphodiester linkages at the anomeric position are by virtue of the substitution positions different than the phosphodiester linkages in nucleic acids. This fact and the conformation and dynamics of a phosphodiester linked repeating unit versus the conformation of this building block when present in the biopolymer prompted us to perform molecular dynamics simulations of the repeating units in the CPS from *H. influenzae* types c and f. Furthermore, results from simulation are compared to experimental NMR data on the CPS in solution.

Materials and Methods

General. The phosphodiester-linked disaccharide α-D-Gal*p*-(1-OPO_2^--4)-*β*-D-Glc*p*NAc3Ac-OMe is denoted by ***c*** and α-D-Gal*p*NAc3Ac−(1-OPO_2^--3)-*β*-D-Gal*p*NAc-OMe by ***f***. Atoms in the terminal α-linked residues are denoted by a prime. The torsion angles at the phosphodiester linkage are denoted by ϕ = H1′−C1′−O1′−P, ζ = C1′−O1′−P−OX, α = O1′−P−OX-CX, and ψ = P−OX-CX-HX, where X is the substitution position. The pD of CPS solutions in D_2O was adjusted by NaOD/D_2O to ∼7. ^{31}P and ^{1}H NMR measurements were performed at 30 °C using Varian 400 and 600 NMR spectrometers, respectively. Determination of $^3J_{H,P}$ was performed using direct measurement of peak separation, comparison to spin simulated multiplets using VNMR (Varian), and analysis of the multiplet resonance from the proton at the glycosyloxylated carbon obtained by 1D ^{1}H,^{1}H TOCSY experiments[11] where the H1 resonance was selectively excited as well as by H1′ decoupled ^{31}P NMR spectra.

Simulation. The molecular simulation program CHARMM[12] (parallel version, C25b2) with the force field PARM22 (Molecular Simulation Inc. San Diego, CA) was used for the simulations. Each molecular dynamics run was started with the solvation of a previously energy-minimized ***c*** or ***f*** molecule and a sodium counterion in a well equilibrated cubic water box with a side length of 40.39 Å containing 2197 TIP3P water[13] molecules. Removing the waters that were closer than 2.5 Å to any solute atom resulted in systems with the solute and 2142−2151 waters. The system was then energy-minimized with steepest descent (200 steps), followed by the adopted basis Newton−Raphson method until the root-mean-square gradient was less then 0.01 kcal mol^{-1} Å^{-1}. Subsequent heating was

* Corresponding author. E-mail: gw@organ.su.se.
[†] Department of Organic Chemistry, Stockholm University.
[‡] Division of Physical Chemistry, Stockholm University.

10.1021/jp0041555 CCC: $20.00
Published on Web 06/28/2001

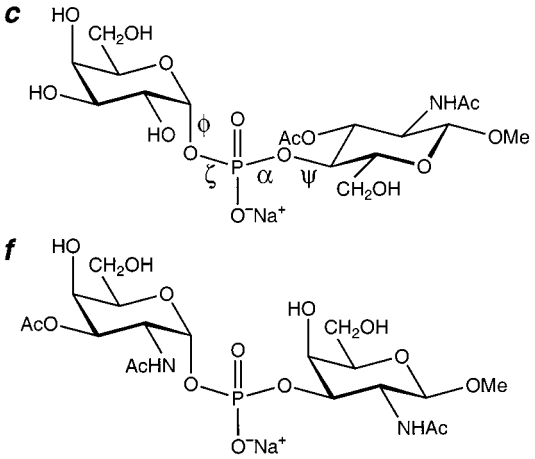

Figure 1. Schematic of the disaccharide repeating units from *H. influenzae* serotype c (top) and f (bottom) CPS investigated as methyl glycosides by MD simulations. In the text, these are referred to as ***c*** and ***f***, respectively.

performed from 100 to 300 K during 8 ps at 5 K increments. Equilibration was performed at 300 K for 200 ps; no drift in temperature or energy was noticed during the last 100 ps. After the equilibration period, 1 ns production runs were performed. Minimum image boundary conditions and a dielectric constant of unity were employed in the simulations. The temperature was kept constant at 300 K using Berendsen's weak-coupling algorithm.[14] Coordinates were saved every 0.2 ps for analysis. SHAKE was used to restrain the hydrogen-heavy atom bond stretch[15] with a tolerance gradient of 10^{-4}. The time step was accordingly set to 2 fs. A heuristic update frequency was used for the nonbond list. The long-range electrostatic interactions were evaluated using either a force shift truncation acting to 18 Å (simulations I and II)[16] or the Ewald summation technique (simulations III and IV),[17,18] with $r_c = 12$ Å, $\kappa = 0.3$ Å^{-1}, and $k^{max} = 9$. The starting conformations of ***c*** and ***f*** were the same in I and III and in II and IV. In total, eight simulations were performed with different initial seeds. The geometric criteria for evaluation of hydrogen bonding was set to an oxygen−hydrogen distance < 2.5 Å and a donor-hydrogen···acceptor angle $\Theta > 135°$. Radial distribution functions (RDF) were integrated for oxygen−oxygen out to 3.5 Å and for hydrogen−oxygen to 2.5 Å to give the corresponding coordination numbers. For the generation of spatial distribution functions (SDF), the molecular reference frame was attached to the C3′−O1′ and C3−O1′ vectors in ***c*** and to the P−O−pro−R_P and P−O−pro−S_P vectors in ***f***. The SDF figures were produced with the simulation software M.Dyna*Mix*[19] and the "gOpenMol" package.[20]

Computations were performed at an IBM SP2 at the Center for Parallel Computers, KTH, Stockholm using 16 nodes. A 100 ps of MD production run employed ∼19 h of CPU time when using the Ewald summation technique and ∼13 h with the force shift truncation procedure.

Results and Discussion

I. Conformation and Flexibility. For the phosphodiester-linked disaccharides (Figure 1), four torsion angles are of interest in describing the three-dimensional structure and the dynamics of the system, viz., ϕ, ζ, α, and ψ. Scatter plots of these torsion angles are shown in Figure 2, from which it is evident that a lower flexibility exists for the torsions closest to the sugar residues, i.e., ϕ and ψ. The two other torsions in the phosphodiester linkage (ζ and α) have a larger mobility. Similar results are obtained from the other simulations, as exemplified by the trajectories in Figures 3 and 4 for ***c*** and ***f***, respectively. The compiled data of the simulations (Table 1) reveal the lowest RMSD values for torsion angle ϕ and similar or somewhat larger values for ψ. The averaged values of the torsions are in the vicinity of 0°, with some shifted slightly positive as well as somewhat negative. Essentially, during these different 1 ns simulations, the torsions are well converged and may be described by a single conformational state or a slightly extended conformational state as for ψ of ***f***. On the contrary, conspicuous trans−gauche or gauche−trans transitions are observed for the two central torsion angles, which also leads to significantly larger RMSD values. In particular, these transitions exhibit correlated motions, as observed in simulation IIC (Figure 3). The behavior of the sodium counterion also differs significantly between simulations. In simulation IIC (Figure 3), the sodium ion stays closely complexed. A small positional change occurs at the time of torsional transitions (after ∼400 ps) described above. In contrast, simulation IF (Figure 4) reveals large translational diffusion of the sodium counterion which populates regions close to the phosphorus atom as well as far away. For the torsion angle averages investigated herein, the choice of truncation method for the long-range electrostatic interaction did not make any major difference. However, the Ewald summation method required approximately 50% more simulation time. These phosphodiester-linked disaccharides represents the simplest building block and one repeating unit of the CPS. The flexibility may be described as lower close to the sugar residues and higher at the phosphorus atom acting as a hinge.

TABLE 1: Torsion Angle Results from MD Simulations (I and II,: Force Shift Truncation; III and IV, Ewald Summation)

simulation	ϕ (°)	ζ (°)	α (°)	ψ (°)
IC	16 [11][a]	−178 [20]	−25 [42]	−1 [10]
IIC	14 [10]	111 [49]	136 [59]	1 [9]
IIIC	17 [11]	−178 [19]	39 [35]	1 [10]
IVC	17 [12]	−13 [66]	−169 [41]	−3 [12]
IF	5 [10]	−152 [40]	1 [57]	−20 [22]
IIF	5 [10]	−138 [45]	31 [30]	−17 [21]
IIIF	6 [10]	−115 [45]	115 [64]	−19 [23]
IVF	4 [10]	−67 [42]	−133 [80]	−28 [26]

[a] Root-mean-square deviation in square brackets.

TABLE 2: Comparison of *J* Couplings (Hz) from NMR Experiment and MD Simulations

	experiment[a]	simulation[c]
$^3J_{H1',P}$ (type c)	6.4 [0.1][b]	9.5 (0.2)[d]
$^3J_{H4,P}$ (type c)	9.0 [0.5]	10.4 (0.1)
$^3J_{H1',P}$ (type f)	7.0 [0.1]	10.4 (0.1)
$^3J_{H3,P}$ (type f)	9.0 [0.5]	8.4 (0.9)

[a] Measured on the CPS. [b] Estimated error in square brackets. [c] Average of the four simulations of each type. [d] Standard deviation in parentheses.

II. NMR Experiments. The structures of the CPS of both serotypes have previously been determined by NMR spectroscopy. In Table 2, we report the $^3J_{H,P}$ values of the CPS determined in this study. The Karplus-type relationship for this scalar coupling interaction has been described by[21]

$$^3J_{POCH} = 15.3 \cos^2\theta - 6.1 \cos\theta + 1.6 \qquad (1)$$

where θ is the torsion angle. In the present study, we limit the analysis to the scalar couplings from phosphorus related to protons, although a full analysis including spin−spin couplings to carbons is possible[22] but does not necessarily reveal

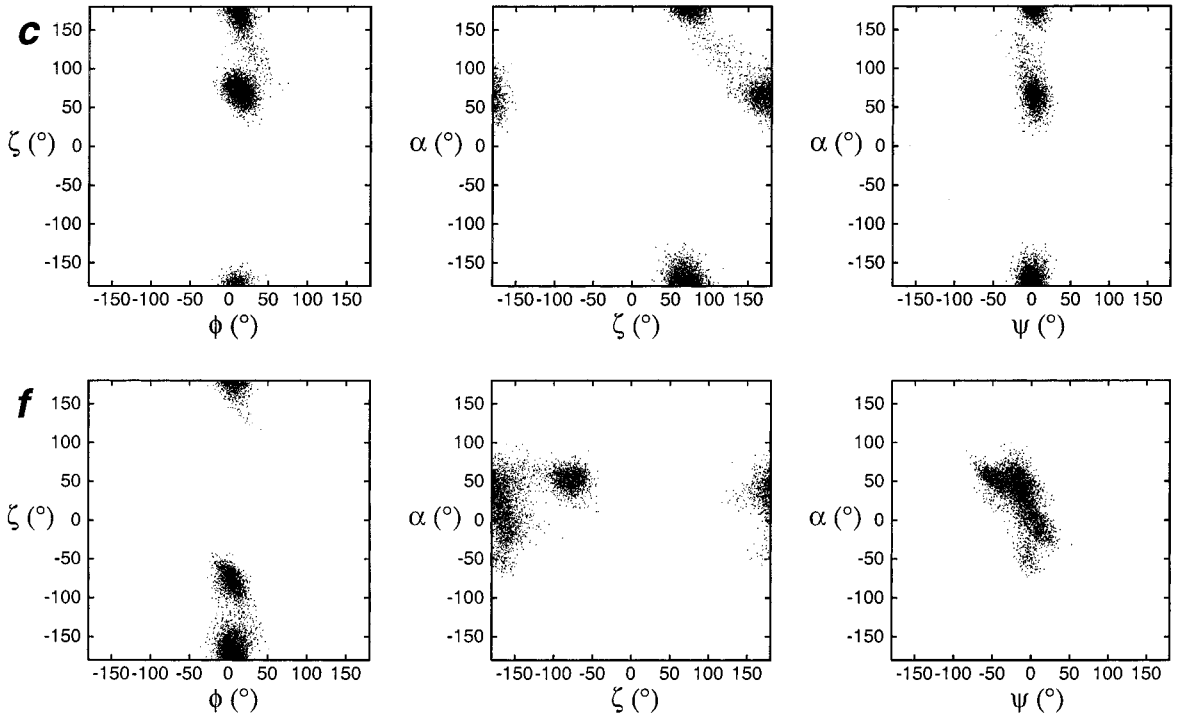

Figure 2. MD scatter plots of torsion angles at the phosphodiester linkage from simulation IC (upper row) and simulation IVF (lower row).

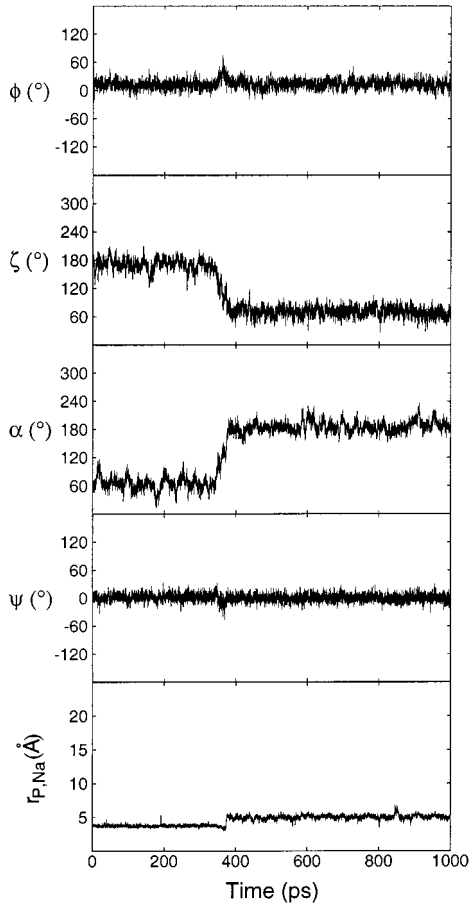

Figure 3. Molecular dynamics trajectories of ***c*** from simulation IIC showing torsion angles at the phosphodiester linkage as well as the distance from phosphorus to the sodium counterion (bottom panel).

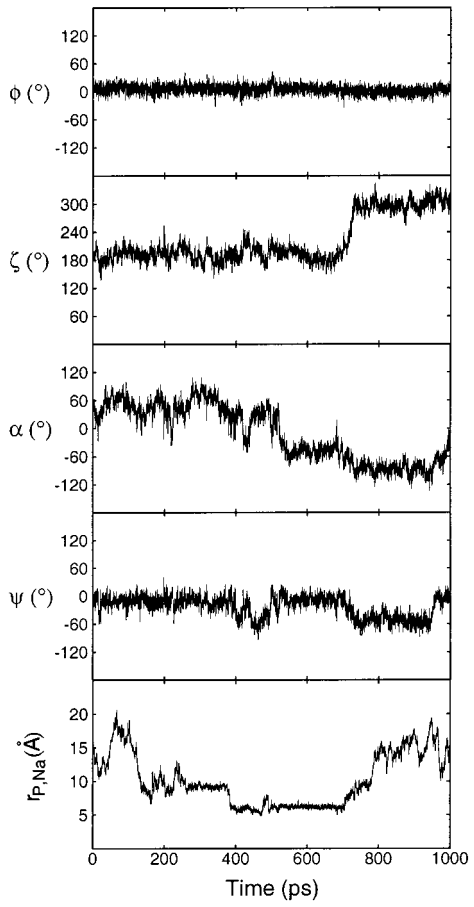

Figure 4. MD trajectories of ***f*** from simulation IF showing torsion angles at the phosphodiester linkage and the distance from phosphorus to the sodium counterion (cf. Figure 3).

substantially greater insight in the present case. The $^3J_{H1',P}$ scalar couplings related to the ϕ torsion angles of the CPS are ~7 Hz, whereas those related to the ψ torsion angles are ~9 Hz. Recently, $^3J_{H1',P}$ values in oligosaccharides with one phosphodiester-linkage were reported and showed 6.6 Hz for serotype c and 7.3 Hz for serotype f.[23] Thus, for this torsion angle the

TABLE 3: Hydrogen Bonds and Coordination Numbers from Simulation IVC

atom	acceptor	donor	total	n_{OO}	n_{OH}	n_{HO}	n_H
O1	0.39	−	0.39	2.12	1.03	−	1.03
N2	0.01	0.43	0.44	1.65	0.03	0.87	0.90
O2Am	0.76	−	0.76	3.62	2.18	−	2.18
O3	0.43	−	0.43	1.26	1.06	−	1.06
O3Ac	0.63	−	0.63	3.14	1.64	−	1.64
O4	0.19	−	0.19	0.98	0.46	−	0.46
O5	0.19	−	0.19	1.21	0.43	−	0.43
O6	0.89	0.31	1.20	4.07	1.92	0.80	2.72
O1′	0.54	−	0.54	1.56	0.96	−	0.96
O2′	0.83	0.17	1.00	3.02	1.71	0.41	2.12
O3′	0.64	0.46	1.10	3.93	1.55	0.90	2.45
O4′	0.70	0.49	1.19	3.42	1.51	0.84	2.35
O5′	0.66	−	0.66	2.24	1.42	−	1.42
O6′	0.93	0.41	1.34	4.27	1.96	0.83	2.79
O−pro−R_P	1.44	−	1.44	3.32	2.46	−	2.46
O−pro−S_P	1.30	−	1.30	3.46	2.55	−	2.55

TABLE 4: Hydrogen Bonds and Coordination Numbers from Simulation IVF

atom	acceptor	donor	total	n_{OO}	n_{OH}	n_{HO}	n_H
O1	0.24	−	0.24	2.09	1.04	−	1.04
N2	0.01	0.32	0.33	1.41	0.05	0.71	0.76
O2Am	0.64	−	0.64	3.54	2.27	−	2.27
O3	0.21	−	0.21	1.48	0.72	−	0.72
O4	0.47	0.23	0.70	3.26	0.74	0.72	1.46
O5	0.16	−	0.16	1.42	0.74	−	0.74
O6	0.52	0.17	0.69	4.07	1.90	0.79	2.70
O1′	0.23	−	0.23	1.40	0.69	−	0.69
N2′	0.01	0.12	0.13	0.86	0.06	0.28	0.34
O2Am′	0.81	−	0.81	3.35	2.15	−	2.15
O3′	0.32	−	0.32	1.51	0.75	−	0.75
O3Ac′	0.50	−	0.50	3.39	1.60	−	1.60
O4′	0.67	0.29	0.96	3.59	1.77	0.84	2.61
O5′	0.50	−	0.50	2.28	1.58	−	1.58
O6′	0.66	0.29	0.95	4.14	1.92	0.85	2.77
O−pro−R_P	0.89	−	0.89	2.67	1.89	−	1.89
O−pro−S_P	1.05	−	1.05	3.79	2.50	−	2.50

conformational difference is negligible between oligomer and CPS, as revealed by the $^3J_{H1',P}$ values.

From the MD simulations the $^3J_{H,P}$ values were calculated (Table 2). The spin−spin couplings related to the ϕ torsion angles are overestimated by ∼3 Hz, whereas those related to the ψ torsion angles differ by only ∼1 Hz. However, taking into account the shape of the Karplus curve these differences translates to conformational shifts of ∼20° for ϕ and ∼10° ψ. Thus, the models representing one repeating unit of the CPS should for these torsion angles be similar to the conformation of the CPS.

Recently, an MD and NMR study was presented of the CPS from serotype b, which contains a ribitol phosphodiester in the repeating unit. Good agreement was found between NMR observables and the MD simulation which used the GROMOS force field.[24]

III. Solvent Structure. The characteristic intermolecular solute−solvent hydrogen bonds are exemplified from one simulation each of ***c*** and ***f*** in Tables 3 and 4, respectively. The highest donation to solvent is present for O4′ in a region of the molecules sufficiently far away from the phosphodiester linkage. The oxygens linked to phosphorus but not to the sugar residues, i.e., O−pro−R_P and O−pro−S_P, show the largest degree hydrogen bond formation as acceptors from water. The lowest hydrogen bond donors are present close to the glycosidic linkage, i.e., O2′ in ***c*** and N2′ in ***f***.

The solvent structure around a solute has been studied using radial distribution functions (RDF) of atom density given by

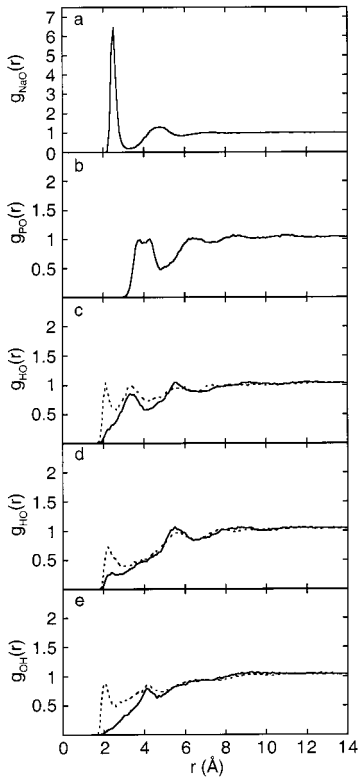

Figure 5. Radial distribution functions from simulations: (a) $g_{NaO}(r)$ from simulation IVF; (b) $g_{PO}(r)$ from simulation IVC; (c) $g_{HO}(r)$ from simulation IIIC around O2′ (solid line) and O3′ (dashed line); (d) $g_{HO}(r)$ from simulation IVF around N2′ (solid line) and N2 (dashed line); (e) $g_{OH}(r)$ from simulation IIC around the carbonyl oxygen in the *O*-acetyl group (O3Ac) averaged over 400−1000 ps (solid line) and 0−350 ps (dashed line).

$$g_{AB}(r) = \frac{\rho_B(r|r_A = 0)}{\rho_B} \tag{2}$$

where the first index A refers to a solute atom at the origin and the second index B refers to a solvent atom B, r is the distance between the atoms, and ρ_B is the bulk density of B in the solvent. Five types of RDFs were calculated, namely, $g_{OO}(r)$, $g_{OH}(r)$, $g_{HO}(r)$, $g_{PO}(r)$, and $g_{NaO}(r)$. Coordination numbers were obtained by integration of $g_{AB}(r)$ out to the first minimum (Tables 3 and 4).

In simulation IVF $g_{NaO}(r)$ shows a pronounced first maximum at 2.5 Å (Figure 5a). A large coordination number n_{NaO} of 6.0 is subsequently observed. The $g_{PO}(r)$ in Figure 5b reveals a typical and quite broad first maximum peak. A shielding from hydrogen bonding to solvent is present for HO2′ compared to HO3′ (Figure 5c) and HN2′ compared to HN2 (Figure 5d) since the first maximum is essentially absent for the former in these comparisons. These results are consistent with the low coordination numbers n_{HO} (Tables 3 and 4). In simulation IIC, a transition occurred around 400 ps which was accompanied by a change in the distance between the phosphorus atom and sodium (vide supra). Analysis of the RDF prior to and after the transition (Figure 5e) shows that the carbonyl oxygen of the *O*-acetyl group becomes inaccessible to hydrogen bond donation from solvent after the transition takes place.

Intramolecular hydrogen bonds were present in ***c*** for HO2′ to O−pro−S_P 51% of the time in simulations IC and IIIC and to O−pro−R_P 24% in simulation IVC. In ***f***, HN2′ showed intramolecular hydrogen bonding to one of the prochiral oxygens linked to phosphorus 30 ± 10% in all of the four simulations.

Thus, the above analyzed data can be explained by a quite large degree of internal hydrogen bonding from the terminal sugar residue to an oxygen atom in the phosphodiester linkage. Also, some water bridges were consistently observed in all simulations, viz., O1′−O5′ (11% in ***c*** and 7% in ***f***), O5′−HO6′ (7% in ***c*** and 5% in ***f***), and between the prochiral oxygens linked to phosphorus (6% in ***c*** and 5% in ***f***). Also, for ***c***, the O1′−HO6′ pair was bridged by a water molecule in the four simulations 8% of the time.

Further information about the three-dimensional solvation structure can be obtained using different averaging techniques.[25−29] In this study, we employ spatial distribution functions (SDF) of atomic density around a solute[30] given by

$$g_{AB}(\vec{r}) = \frac{\rho_B(\vec{r}\,|\,\vec{r}_A = 0)}{\rho_B} \qquad (3)$$

where, similar to eq 2, the first index A refers to a solute atom and the second index B refers to a solvent atom, $\vec{r}$ is a vector in Cartesian coordinate space between the atoms, and ρ_B is the bulk solvent density of B in the solvent. The SDFs give both the radial and angular dependence of the solvation structure around a solute fixed in the local coordinate system. Calculation of the SDFs can be done in a similar way as the RDFs during the simulations. In the case of large and flexible molecules, it may be difficult to create the local frame due to excessive intramolecular and conformational fluctuations as the simulation proceeds. Since the SDFs are four-dimensional quantities, the visualization requires special attention. Usually, one of the dimensions is removed by using either a projection onto two Cartesian dimensions or isodensity surfaces of the SDF intensities, displayed in three dimensions as presented here.

The SDFs of ***c*** and ***f*** are shown in Figure 6. In the former case, it was possible to create the molecular reference frame from atoms in both sugar rings and still produce an informative SDF over the trajectory part analyzed. However, in the latter case, the flexibility both within a conformational state and transitions of the torsion angle ψ in ***f*** (vide supra) led to a molecular reference frame at the phosphodiester group. In ***c***, a band-shaped region is revealed between the phosphorus and O5′ (middle of picture). A circular band-shaped solvation shell is also indicated for ***f***. These patterns are typical for water solutions and were also observed in our previous simulations.[31] The hydrated sodium ion is quite well-defined close to ***c***, whereas it seems more difficult for it to find a well-defined coordination position near ***f***. Interestingly, a water molecule in hydrogen bond donation to O−pro−S_P in ***c*** is evident from the SDF (lower part of picture). The differences in the SDFs of ***c*** and ***f*** reveal both the strengths, i.e., the information content, and the difficulties in reducing the dimensionality of a dynamic system in order to obtain a static graphical visualization thereof.

IV. Comparison to Nucleic Acids. Analogous to the repeating units of the *H. influenzae* types c and f CPS are the nucleic acids with their repeating phosphodiester−sugar backbone. On the basis of computer simulations, a very detailed picture of hydration structure around nucleic acids and nucleoides has been obtained.[32−34] Conformations of nucleotides depend totally on seven torsion angles, which together specify the secondary structure of nucleic acids. The sugar−phosphate backbone is characterized by six torsion angles (denoted as α, β, γ, δ, ϵ, and ζ) in 5′ to 3′ order starting from O3′−P−O5′−C5′, while the orientation of the base relative to the sugar pucker is specified by the seventh, glycosidic torsion angle χ. Also, the puckering conformations of the five-membered furanose sugar ring and its pseudorotation cycle are described by five additional torsion angles.

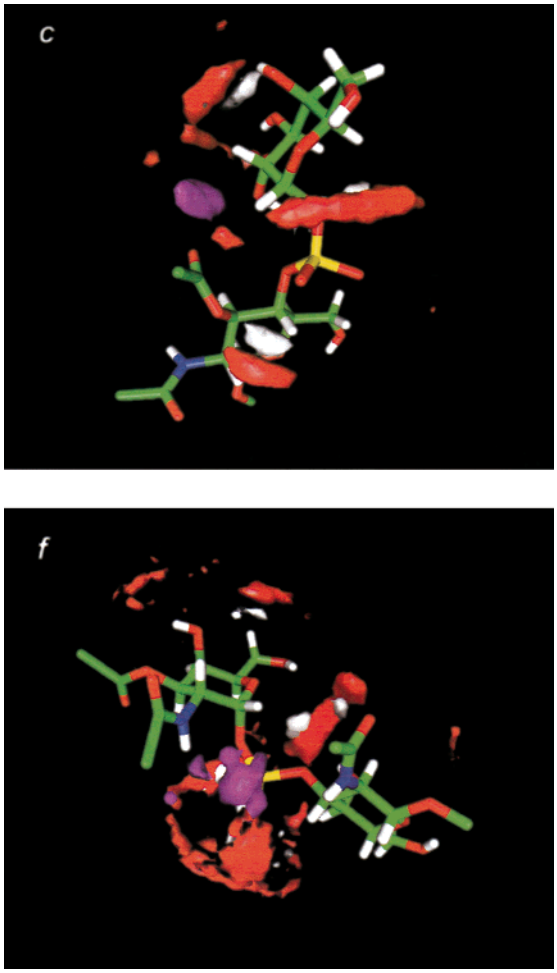

Figure 6. Spatial distribution functions around disaccharides ***c*** (simulation IIC, 400−1000 ps) and ***f*** (simulation IVF, 200−1000 ps). Contours show the regions of high positive deviations of the local density. These were 6, 5, and 10000 times higher in ***c*** than the average value for oxygen, hydrogen, and sodium, respectively, and 4, 3, and 600 times higher in ***f***, correspondingly. Atomic coloring is green for carbon, red for oxygen, white for hydrogen, yellow for phosphorus, and purple for sodium.

From the point of view of the structure of nucleic acids, it is the torsion about the C4′−C5′ bond (γ) which is of crucial importance in positioning the phosphate group relative to the adjacent sugar and base. However, there is no analogue to this particular torsion angle, containing a methylene group along the linkage, in the CPS backbone. In comparing the internal structure of polynucleotides or nucleic acids to that of the polysaccharide, we can inspect the two torsion angles α and ζ about the two bonds containing the phosphorus atom (see Figure 1). The electronic structure of the phosphate group is important with the vacant d-orbitals of phosphorus being used in forming the hybridized orbitals affecting these two torsion angles.[35] In general, for single-stranded polynucleotides, the gauche effect limits the α torsion angle to −sc (around −90°) and the ζ torsion angle to −sc or ap (∼180°) in the so-called Klyne−Prelog notation. In helical structures with the bases paired, only the −sc conformation is allowed for both α and ζ. For example, our recent MD simulation study of B-DNA in water solution[36] shows a clear population maximum around −90° with scattered minor distributions around 180° for both α and ζ.

X-ray structures of tRNA and DNA oligomers can give some information about characteristic features of torsion angles

involving P−O bonds. For example, rather than an extended W-conformation, a skewed conformation is found for the C−O−P−O−C fragment in simpler polynucleotides. This is normally explained by the gauche effect, originating from the oxygen lone-pair being able to donate electrons to the polarized P−O bond.[35] From the α versus ζ Ramachandran scatter plots (middle of Figure 2), we can observe that the helical region for nucleic acids with $\alpha = \zeta = -90°$ is completely absent. Thus, only conformations found in simple phosphodiesters[35] agree with the regions found to be populated in the present simulations of single repeating units of the CPS. However, the indication of parts of circular band-shaped solvation shells in ***c*** and ***f*** is a pattern even more characteristic in the hydration of double-helix B-DNA structures.[34]

Conclusions

The flexibility in the phosphodiester linked disaccharides of the repeating units of *H. influenzae* types c and f were of limited magnitude during the 1 ns molecular dynamics simulations for the torsion angles close to the sugar residues, whereas for the torsions at the phosphorus atoms, major transitions occurred. $^3J_{H,P}$ measured on CPS material were used for comparison to simulated data. Only small changes in torsion angles of the model disaccharides are required in order to fulfill $^3J_{H,P}$ in the polymers. The solvent structure around the disaccharides were investigated by hydrogen bond analysis as well as radial and spatial distribution functions. Specific intramolecular hydrogen bonding and regions where ordered solvent molecules reside were found.

Acknowledgment. This work was supported by grants from the Swedish Natural Science Research Council. We thank Dr. R. Schneerson, Bethesda, for kindly providing us with polysaccharide samples and the Center for Parallel Computers, KTH, Stockholm, for putting computer facilities at our disposal.

References and Notes

(1) Kenne, L.; Lindberg, B. In *The Polysaccharides*; Aspinall, G. O., Ed.; Academic Press: New York, 1983; Vol. 2, pp 287−363.
(2) Egan, W.; Schneerson, R.; Werner, K. E.; Zon, G. *J. Am. Chem. Soc.* **1982**, *104*, 2898−2910.
(3) Barbour, M. L.; Mayon-White, R. T.; Coles, C.; Crook, D. W. M.; Moxon, E. R. *J. Infect. Dis.* **1995**, *171*, 93−98.
(4) Campagnari, A. A.; Gupta, M. R.; Dudas, K. C.; Murphy, T. F.; Apicella, M. A. *Infect. Immun.* **1987**, *55*, 882−887.
(5) Brandefors-Helander, P.; Classon, B.; Kenne, L.; Lindberg, B. *Carbohydr. Res.* **1979**, *76*, 197−202.
(6) Egan, W.; Tsui, F.-P.; Climenson, P. A.; Schneerson, R. *Carbohydr. Res.* **1980**, *80*, 305−316.
(7) Egan, W.; Tsui, F.-P.; Schneerson, R. *Carbohydr. Res.* **1980**, *79*, 271−277.
(8) Brandefors-Helander, P.; Kenne, L.; Lindqvist, B. *Carbohydr. Res.* **1980**, *79*, 308−312.
(9) Jansson, P.-E.; Lindberg, J.; Wimalasiri, K. M. S.; Henrichsen, J. *Carbohydr. Res.* **1991**, *217*, 171−180.
(10) Linnerborg, M.; Weintraub, A.; Widmalm, G. *Carbohydr. Res.* **1999**, *320*, 200−208.
(11) Kessler, H.; Oschkinat, H.; Griesinger, C. *J. Magn. Reson.* **1986**, *70*, 106−133.
(12) Brooks, B. R.; Bruccoleri, R. E.; Olafson, B. D.; States, D. J.; Swaminathan, S.; Karplus, M. *J. Comput. Chem.* **1983**, *4*, 187−217.
(13) Jorgensen, W. L.; Chandrasekhar, J.; Madura, J. D.; Impey, R. W.; Klein, M. L. J. *J. Chem. Phys.* **1983**, *79*, 926−935.
(14) Berendsen, H. J. C.; Postma, J. P. M.; van Gunsteren, W. F.; DiNola, A.; Haak, J. R. *J. Chem. Phys.* **1984**, *81*, 3684−3690.
(15) Ryckaert, J. P.; Ciccotti, G.; Berendsen, H. J. C. *J. Comput. Phys.* **1977**, *23*, 327−341.
(16) Steinbach, P. J.; Brooks, B. R. *J. Comput. Chem.* **1994**, *15*, 667−683.
(17) Ewald, P. *Ann. Phys.* **1921**, *64*, 253−287.
(18) Feller, S. E.; Pastor, R. W.; Rojnuckarin, A.; Bogusz, S.; Brooks, B. R. *J. Phys. Chem.* **1996**, *100*, 17011−17020.
(19) Lyubartsev, A.; Laaksonen, A. *Comput. Phys. Commun.* **2000**, *128*, 565−589.
(20) Laaksonen, L. *gOpenMol*, version 1.31; Center of Scientific Computations: Espoo, Finland, 1999 (http://laaksonen.csc.fi/gopenmol/gopenmol.html).
(21) Lankhorst, P. P.; Haasnoot, C. A. G.; Erkelens, C.; Altona, C. *J. Biomol. Struct. Dyn.* **1984**, *1*, 1387−1405.
(22) Bernlind, C.; Oscarson, S.; Widmalm, G. *Carbohydr. Res.* **1994**, *263*, 173−180.
(23) Hansson, J.; Oscarson, S. *J. Org. Chem.*, submitted for publication.
(24) Maestre, M.; Pérez, C. S. *Magn. Reson. Chem.* **2000**, *38*, 123−125.
(25) Schmidt, R. K.; Karplus, M.; Brady, J. W. *J. Am. Chem. Soc.* **1996**, *118*, 541−546.
(26) Liu, Q.; Brady, J. W. *J. Am. Chem. Soc.* **1996**, *118*, 12276−12286.
(27) Liu, Q.; Schmidt, R. K.; Karplus, P. A.; Brady, J. W. *J. Am. Chem. Soc.* **1997**, *118*, 7851−7862.
(28) Sidhu, K. S.; Goodfellow, J. M.; Turner, J. Z. *J. Chem. Phys.* **1999**, *110*, 7943−7950.
(29) Andersson, C.; Engelsen, S. B. *J. Mol. Graphics Modell.* **1999**, *17*, 101−105, 131−133.
(30) Kusalik, P. G.; Laaksonen, A.; Svishchev, I. M. In *Molecular Dynamics: From Classical to Quantum Methods*; Balbuena, P. B., Seminario, J. M., Eds.; Elsevier Science: Amsterdam, 1999; Theoretical and Computational Chemistry Vol. 7, pp 61−97.
(31) Vishnyakov, A.; Widmalm, G.; Kowalewski, J.; Laaksonen, A. *J. Am. Chem. Soc.* **1999**, *121*, 5403−5412.
(32) Young, M. A.; Ravishanker, G.; Beveridge, D. L. *Biophys. J.* **1997**, *73*, 2313−2336.
(33) Feig, M.; Pettitt, B. M. *J. Mol. Biol.* **1999**, *286*, 1075−1095.
(34) Lyubartsev, A. P.; Laaksonen, A. *J. Biomol. Struct. Dyn.* **1998**, *16*, 579−592.
(35) Saenger, W. *Principles of Nucleic Acid Structure*; Springer: New York, 1984.
(36) Lohikoski, R. A.; Timonen, J.; Lyubartsev, A. P.; Laaksonen, A. *Mol. Simul.*, in press.